Molecular Pharmacology Fast Forward. Published on May 11, 2016 as DOI: 10.1124/mol.116.104190
This article has not been copyedited and formatted. The final version may differ from this version.

Cryo-EM analysis of the conformational landscape of human P-glycoprotein (ABCB1) during its catalytic cycle

Gabriel A. Frank, Suneet Shukla, Prashant Rao, Mario J. Borgnia, Alberto Bartesaghi, Alan Merk, Aerfa Mobin, Lothar Esser, Lesley A. Earl, Michael M. Gottesman, Di Xia, Suresh V. Ambudkar, and Sriram Subramaniam

Laboratory of Cell Biology, Center for Cancer Research, National Cancer Institute, National Institutes of Health, Bethesda, MD 20892, USA (GAF, SSh, PR, MJB, AB, AMe, AMo, LE, LAE, MMG, DX, SVA, SSu)

Molecular Pharmacology Fast Forward. Published on May 11, 2016 as DOI: 10.1124/mol.116.104190
This article has not been copyedited and formatted. The final version may differ from this version.

Running title: Cryo-EM analysis of the human P-glycoprotein ATPase cycle

Corresponding Authors: Suresh V. Ambudkar and Sriram Subramaniam

50 South Drive, Rm 4306, MSC 8008

Bethesda, MD 20892

Ph: 301-594-2062 (SSu) and 301-402-4178 (SVA)

Email: ss1@nih.gov (SSu) and ambudkar@helix.nih.gov (SVA)

Text pages: 14

Tables: 0, 1 supplemental

Figures: 4, 2 supplemental

References: 37

Abstract: 150 words

Introduction: 538 words

Discussion: 575 words

Abbreviations: cryo-EM (cryo-electron microscopy); DDM (dodecyl maltoside); hP-gp (human P-glycoprotein); NBDs (nucleotide binding domains); P-gp (P-glycoprotein); TMD (transmembrane domain); Vi (sodium orthovanadate); WT (wild-type)

Molecular Pharmacology Fast Forward. Published on May 11, 2016 as DOI: 10.1124/mol.116.104190
This article has not been copyedited and formatted. The final version may differ from this version.

Abstract

The multidrug transporter P-glycoprotein (P-gp, ABCB1) is an ATP-dependent efflux pump that mediates the efflux of structurally diverse drugs and xenobiotics across cell membranes, affecting drug pharmacokinetics and contributing to the development of multidrug resistance. Structural information about the conformational changes in human P-gp during the ATP hydrolysis cycle has not been directly demonstrated, although mechanistic information has been inferred from biochemical and biophysical studies done with P-gp and its orthologs, or from structures of other ABC transporters. Using single particle cryo-electron microscopy, we report the surprising discovery that, in the absence of the transport substrate and nucleotides, human P-gp can exist in both open (nucleotide-binding-domains (NBDs) apart; inward-facing) and closed (NBDs close; outward-facing) conformations. We also probe conformational states of human P-gp during the catalytic cycle, and demonstrate that following ATP hydrolysis, P-gp transitions through a complete closed conformation to a complete open conformation in the presence of ADP.

Molecular Pharmacology Fast Forward. Published on May 11, 2016 as DOI: 10.1124/mol.116.104190
This article has not been copyedited and formatted. The final version may differ from this version.

Introduction

P-glycoprotein (P-gp) is a member of the ATP-binding cassette (ABC) protein superfamily, which mediates the detoxification of cells in an ATP-dependent fashion by exporting a wide range of structurally dissimilar compounds across the plasma membrane (Ambudkar et al., 1999). ABC transporters share common structural features: they have a symmetric or pseudo-symmetric structure, with two transmembrane domains (TMDs) and two nucleotide-binding domains (NBDs) (Wilkens, 2015). Binding and hydrolysis of ATP is mediated by the NBDs; ATP binding has generally been thought to bring the NBDs into close proximity, although this has not been demonstrated structurally.

A common theme of efflux by ABC transporters is that ATP hydrolysis at the interface of NBDs is required for transition between an inward-facing conformation (which allows drug/ substrate binding to a cytoplasmically accessible pocket between the TMDs) and an outward-facing conformation (which would then allow release of the substrate to the extracellular space) (Wilkens, 2015). ATP hydrolysis is known to require the "closure" of the NBDs, where both arms of the cytoplasmic domain come into close contact; the rate-limiting step of this reaction is the release of ADP post-hydrolysis (Kerr et al., 2001). While the presence of certain substrates can impact the rate of ATP hydrolysis, human P-gp has a significant basal ATPase activity in the absence of any substrate (Loo et al., 2012; Ramachandra et al., 1996). Thus while ATPase activity is required for drug transport, the presence or absence of substrate does not alter the fundamental conformational changes involved in ATPase activity.

Molecular Pharmacology Fast Forward. Published on May 11, 2016 as DOI: 10.1124/mol.116.104190
This article has not been copyedited and formatted. The final version may differ from this version.

Although several structures of both eukaryotic and prokaryotic ABC transporters have been reported using X-ray crystallography (Aller et al., 2009; Choudhury et al., 2014; Dawson and Locher, 2006; Jin et al., 2012; Perez et al., 2015), the majority of these structures are found in the open, inward-facing conformation, and no matched outward-facing or closed conformations of any single eukaryotic ABC transporter family member has been reported yet. Because of this, the structural mechanisms underlying either the ATPase activity or the transport activity of P-gp are not adequately defined. An additional layer of complexity arises from the fact that P-gp is highly conformationally flexible, with large movements of the NBD arms in the course of the reaction cycle, making it challenging to determine the range of functionally relevant conformations using X-ray crystallography (Aller et al., 2009; Moeller et al., 2015; Szewczyk et al., 2015; Ward et al., 2013).

In this study, we used cryo-electron microscopy (cryo-EM) to evaluate the conformations of human P-gp (hP-gp) in each distinct state of its ATPase cycle. Since P-gp exhibits basal ATPase activity, we evaluated hP-gp conformations at four different points in the ATPase cycle in the absence of any added substrates. Despite the low resolution of the cryo-EM density maps, likely originating from the flexible nature of P-gp, we observed that hP-gp in its apo state can co-exist in two conformations where the NBDs are either separated (resembling what is likely an inward-facing conformation) or in close proximity (resembling a probable outward-facing conformation). These co-existing conformations are present even in the presence of bound ATP prior to hydrolysis, while post-hydrolysis, the transporter sequentially transitions through outward-facing and inward-facing states that correspond to conformations before, and after release of phosphate from the active site, respectively.

Molecular Pharmacology Fast Forward. Published on May 11, 2016 as DOI: 10.1124/mol.116.104190
This article has not been copyedited and formatted. The final version may differ from this version.

Materials and Methods:

Purification of Human P-gp from High-Five insect cells: Crude membranes from High Five insect cells expressing WT-hP-gp, or its double mutant EQ-hP-gp (E556Q/E1201Q), with a 6-histidine tag at the C-terminal end were isolated as described previously (Kerr et al., 2001). The membranes (150-250 mg protein) were solubilized by using 2% n-Dodecyl β-D-maltoside (DDM) in a buffer containing 10 mM Tris-HCl pH 7.5, 150 mM NaCl, 15% glycerol, 5 mM β-mercaptoethanol, 20 mM imidazole and UltraCruz EDTA-free protease inhibitor cocktail tablets (Santa Cruz Biotechnology, Dallas, TX). The solubilized extract was centrifuged at 38,000 rpm (Beckman Ti-45 rotor) for 45 min at 4°C. The supernatant was incubated with Ni-NTA resin (Qiagen Inc., Valencia, CA) pre-equilibrated in solubilization buffer with 0.09% DDM for 14-16 h at 4°C. The beads were washed and P-gp was eluted with the same buffer containing 300 mM imidazole. Fab isolated from UIC2 monoclonal antibody was then added at a molar concentration of P-gp: Fab (3:1) and incubated at 4°C for 15 min. The hP-gp-Fab complex was centrifuged at 300,000xg for 45 min. The complex formation was evaluated on Native PAGE 4-16% Bis-Tris protein gels (Figure 1A, B).

Purification of Fab from UIC2 monoclonal antibody: The hybridoma (UIC2/A) producing the UIC2 monoclonal antibody directed against an extracellular domain of a cell surface hP-gp was obtained from Dr. Eugene Mechetner (Mechetner et al., 1997). UIC2 mAb was produced from this hybridoma as described previously (Mechetner et al., 1997). Fab fragments were isolated using a Fab Preparation Kit (Thermo Fisher Scientific, Waltham, MA) according to instructions provided by the manufacturer. The purity and the yield of the Fab fragment was evaluated by separating purified Fab on 4-16% Bis-Tris protein gel under reducing and non-reducing conditions followed by staining with colloidal blue stain.

Molecular Pharmacology Fast Forward. Published on May 11, 2016 as DOI: 10.1124/mol.116.104190
This article has not been copyedited and formatted. The final version may differ from this version.

Grid preparation for cryo-electron microscopy: 2.5 µL of UIC2 Fab-bound hP-gp solution (2 - 4 mg/ml) in the absence or presence of nucleotides and where appropriate, with 0.3 mM sodium orthovanadate, was deposited on plasma cleaned Quantifoil TEM grids (Quantifoil, Jena, Germany). Blotting of excess liquid and plunge-freezing into liquid ethane were performed with a Leica EM GP (Leica Microsystems, Wetzlar, Germany) set to a blotting time of 3-5 sec and 95 % humidity. Frozen specimens were stored under liquid nitrogen until they were used for imaging.

Data acquisition: Electron micrographs were collected using a Titan Krios electron microscope equipped with a Falcon II detector (FEI Company, Hillsboro, OR). Specimens were imaged at a nominal magnification of 47,000x, corresponding to a pixel size of 1.41 Å at the specimen plane. Micrographs were acquired automatically with the data collection software EPU (FEI Company, Hillsboro, OR) spanning a defocus range of -1.5 to -2.5 µm, at a total dose of ~70 e-/Å^2 distributed over 7 intermediate frames.

Image processing: Drifts and beam-induced motion were compensated by iterative alignment of the intermediate frames using an expectation-maximization algorithm as previously described (Bartesaghi et al., 2014). The program CTFFIND3 was used to estimate contrast transfer function parameters (Mindell and Grigorieff, 2003). Micrographs were selected by manual inspection and particles were picked semi-automatically by cross correlation of the images with a Gaussian disk with a radius of 110 Å followed by search for local maxima. The particles were extracted in a box size of 224×224 pixels and classified into 2D classes using reference free 2D classification (Tang et al., 2007). Classes with clear structural features from the EQ-hP-gp mutant in the apo conformation data set were used to generate a *de novo* 3D initial model using EMAN2 (Tang et al., 2007). The clear density of the Fab bound to the extracellular side of the

Molecular Pharmacology Fast Forward. Published on May 11, 2016 as DOI: 10.1124/mol.116.104190
This article has not been copyedited and formatted. The final version may differ from this version.

protein and the distinctive NBD density that resembles the NBDs in crystal structures of ABC transporters validate the initial model. The final model used projection images that only contained the first ~35 $e^-/Å^2$ of the dose, and reconstruction with 3D classification was carried out using the program RELION (version 1.3) (Scheres, 2012). The apo state EQ-hP-gp data was classified with 11, 5, and 3 classes; all other datasets were classified with 5 and 3 classes. In all cases except for the ADP-bound state, the number of classes did not alter the results. In the case of the ADP dataset, an additional class, corresponding to the intermediately open structure, was identified only after classifying with 5 classes, rather than with 3 classes. A summary of the number of particles in each 3D class from each state can be found in Table S1. FSC curves for the EQ apo open and closed structures (those which were used for docking crystal structures) are presented in Supplementary Figure 2A. The orientation distributions of the projection images of all the maps presented in this study are presented in Supplementary Figure 2B-F, indicating well-spread orientation distribution.

Fits of X-ray coordinates into cryo-EM maps

Structures of available X-ray crystallographic models of homologous ABC transporters were fitted to maps from our study using UCSF Chimera (Pettersen et al., 2004). Models used in this study include those of mouse P-gp (PBD 4M1M and 4KSC), *S. aureus* Sav1866 (PDB 2HYD) and *E. coli* McjD (PDB 4PL0). Prior to fitting the X-ray structures, maps were thresholded according to the molecular volume of the protein. The threshold values for our experimentally determined maps were selected based on the volume of the Fab region, which was matched to the X-ray coordinates of the UIC2 crystal structure (Shukla et al., unpublished data). As the cytoplasmic domains in the maps of the open conformations are clearly separated from each other, it is possible to compare the volume of the cytoplasmic regions of the filtered 4M1M

Molecular Pharmacology Fast Forward. Published on May 11, 2016 as DOI: 10.1124/mol.116.104190
This article has not been copyedited and formatted. The final version may differ from this version.

crystal structure with the respective regions in our cryo-EM maps; the thresholds established by analyzing the volume of the Fab region yielded volumes for the cytoplasmic regions that matched those of 4M1M. We then assessed how well each crystal structure model fit our cryo-EM data by computing the percentage of atoms in the crystal structure that lay outside the cryo-EM map threshold (Figure 3).

ATPase assay: Vanadate-sensitive ATP hydrolysis by hP-gp in crude membranes was measured as described previously (Ambudkar, 1998).

Extraction of nucleotide from purified protein: An equal volume of a phenol:chloroform:isoamyl alcohol (25:24:1, v/v) mixture was added to either purified WT-hP-gp (15 μM), purified EQ-hP-gp (15 μM) or 10 μM ATP in elution buffer and vortexed vigorously for 2 min. The aqueous layer was then separated from the organic layer by centrifuging at 13,000 rpm for 5 min at 4ºC. The upper aqueous layer was then resolved using a C18 column (Vydac) at a flow rate of 0.3 ml/min using gradient elution (solvent A:100mM KH_2PO_4, pH 6.0; solvent B: 90% methanol) with absorbance measured at 254 nm as described previously (Kim et al., 2015).

Oxidative Crosslinking of hP-gp using copper sulfate: Crude membranes from High-Five insect cells (50 μg protein in 50 μL of buffer [10 mM Tris-HCl, 150 mM NaCl, pH 7.5]) were incubated with 5 mM ATP (Sigma-Aldrich, St. Louis, MO) and 10 mM $MgCl_2$ in the presence or absence of 0.3 mM vanadate for 10 min at 37°C. $CuSO_4$ (0.5 mM) was then added for various time points ranging from 15 sec to 15 min at 37°C to complete the crosslinking. The reactions were stopped by adding 10 mM N-ethyl maleimide 20 mM EDTA and SDS-PAGE sample buffer without reducing agent. The samples (0.25-0.5 μg protein) were subjected to SDS-PAGE (7% Tris-Acetate gel, Invitrogen) at a constant voltage of 150 V for 2 hours and immunoblot

Molecular Pharmacology Fast Forward. Published on May 11, 2016 as DOI: 10.1124/mol.116.104190
This article has not been copyedited and formatted. The final version may differ from this version.

analysis was performed with P-gp-specific mouse monoclonal antibody C219 (1:2000 dilution) and enhanced chemiluminescence (ECL, GE healthcare).

Results

We carried out cryo-EM studies of hP-gp in each of the four pivotal states in the ATPase cycle: the 'apo', unbound state (P-gp), the pre-hydrolysis ATP-bound state (P-gp•ATP), the post-hydrolytic ADP-trapped state obtained in the presence of vanadate (P-gp•ADP•V_i, equivalent to P-gp•ADP•P_i), and the ADP-bound post P_i release state (P-gp•ADP). Because P-gp is small and pseudosymmetric, it can be challenging to properly assign orientations of particles during cryo-EM analysis. To facilitate more accurate assignment of particle orientations in projection images, we determined structures of the complex of hP-gp and the Fab fragment of the hP-gp-specific monoclonal antibody UIC2, which binds to the extracellular regions of hP-gp (Mechetner et al., 1997), forming a stable complex (hP-gp•UIC2) with purified P-gp (Figures 1A, B). UIC2 has been shown not to affect the ATPase activity of human P-gp (Ritchie et al., 2011), making this a useful tool to determine P-gp structure. Projection electron micrographs of hP-gp dispersed in vitreous ice display a range of orientations including side and top views (Figure 1C).

2D class averages show clear evidence of distinct P-gp conformations with 'front view' classes (Figure 1D) that differ primarily with respect to the proximity of the two NBDs: in one, they are separated with a classical inverted V-shape formation corresponding to the shape of the "inward-facing" conformation of the transporter, while in the other, they are in close contact, with a well connected "bridge" of density between the two NBD arms. These differences were also confirmed with 3D classification, demonstrating the presence of two prominent classes with

Molecular Pharmacology Fast Forward. Published on May 11, 2016 as DOI: 10.1124/mol.116.104190
This article has not been copyedited and formatted. The final version may differ from this version.

roughly similar proportions, consistent with open and closed hP-gp conformations (Figures 1E and F, respectively). To our knowledge, the presence of a closed conformation in the 'apo' (nucleotide- and substrate-free) state where the NBDs are in close contact has not yet been reported for any member of the ABC transporter family.

To verify that the observed closed state conformation was not an artifact due to trapped nucleotides that were carried with P-gp through the purification procedures, purified hP-gp samples (15 μM) were subjected to nucleotide extraction with phenol:chloroform:isoamylalcohol as described previously (Kim et al., 2015); in this analysis, trapped carryover ATP in the purified protein would result in micromolar concentrations of ATP. These chemical analyses established although a micromolar concentrations (10 μM) could be detected in our assay, the concentration of ATP trapped in the purified protein sample was too low to be detected (Supplementary Figure 1A), confirming that the closed conformation can be sampled even in the absence of bound nucleotide.

Because wild-type (WT) hP-gp immediately hydrolyses ATP, to explore the transient, ATP-bound state of hP-gp, we utilized a mutant form of hP-gp, E556Q/E1201Q. In the E556Q/E1201Q mutant, the catalytic glutamate residues within the Walker A domain in both NBDs are substituted with glutamine, resulting in occlusion of ATP in the pre-hydrolytic state (Sauna et al., 2007; Sauna et al., 2006). As observed with WT hP-gp, both open and closed conformations also exist in the apo-state of the EQ hP-gp mutant (Figure 1G, H). The overall shapes of both open and closed conformations of the apo (nucleotide-free) EQ mutant are essentially superimposable with those observed for the WT protein, indicating that the EQ

Molecular Pharmacology Fast Forward. Published on May 11, 2016 as DOI: 10.1124/mol.116.104190
This article has not been copyedited and formatted. The final version may differ from this version.

mutation does not significantly alter the structural landscape of hPgp. Essentially the same mixture of closed and open conformations were observed upon analysis of the EQ mutant in the presence of ATP, providing a structural snapshot of the next step in the reaction cycle, which precedes ATP (the EQ mutant lacks the ability to hydrolyze ATP) (Figure 1I, J). The presence of trapped ATP in the EQ hP-gp under the conditions used for cryo-EM analysis was confirmed by HPLC of the extracted nucleotides from this sample (Supplementary Figure 1B).

Hydrolysis of ATP by P-gp leads to a transient post-hydrolytic state, in which ADP and phosphate remain in the active site. To capture the post-hydrolytic state, WT hP-gp was incubated with ATP and sodium orthovanadate (V_i) at 37°C for 15 min. V_i has been used to arrest hP-gp and other ABC transporters in the nucleotide-trapped transition state (P-gp•ADP•Vi) (Senior, 2011; Urbatsch et al., 1995). This state is known to have low affinity for transport substrates, and has been proposed to be outward-facing (Sauna and Ambudkar, 2000). Our structural analysis of the post-hydrolytic state shows that only the closed conformation with 'bridged' NBDs is present (Figure 2A). In this state, V_i binding enables the ADP generated by hydrolysis to stay bound to the protein. We note that our findings that hP-gp is in a closed conformation in the presence of ATP and V_i under conditions where ATP is hydrolyzed is at variance with a recent report (Moeller et al., 2015) on ABC transporter structures where the closed state for mouse P-gp was not observed under these conditions. It is possible that the use of cryo-EM rather than negative stain, and the higher resolution of our maps may explain our observation of the closed conformation in this step of the P-gp reaction cycle.

Molecular Pharmacology Fast Forward. Published on May 11, 2016 as DOI: 10.1124/mol.116.104190
This article has not been copyedited and formatted. The final version may differ from this version.

To determine the conformation of the post-hydrolytic ADP-bound state of hP-gp, the final step in the cycle, we incubated WT hP-gp with 5 mM ADP and 5 mM $MgCl_2$. Under these conditions, 3D classification revealed several 'open' conformations (Figures 2B-D), suggesting that the presence of ADP prevents closure of the NBDs. While we present only three different density maps for this state, our analysis cannot rule out the existence of a continuum of conformations that are sampled by the transporter in the presence of ADP. To independently test the conformational landscape derived by cryo-EM analysis, we compared the extent of cysteine cross-linking in the presence of ADP with that observed for apo hP-gp. Previous studies have established that under physiologically relevant conditions, the NBDs of P-gp can be cross-linked by a disulfide bond between C431 and C1074, in apo, but not in the ADP•Vi bound state (Supplementary Figure 1C). Additionally, the apo EQ hPgp mutant likewise is amenable to crosslinking, while the ATP-bound form is somewhat less so (Supplementary Figure 1D). The precise conformational mechanism by which C431 and C1074 come into close enough proximity (>5Å) to crosslink is not yet clear, but some level of conformational flexibility seems to be required for this crosslinking to occur. The conformational flexibility of these residues has also been supported by crosslinking in apo conformation with the bifunctional crosslinker M17M, which has a 24 Å linker length (Sim et al., 2013). Evaluation of the relative extent of crosslinking for the apo and ADP-bound conditions for hP-gp over time showed that the $T_{1/2}$ for $CuSO_4$–induced crosslinking of C431 and C1074 in the NBDs changed from 0.65 (+0.20/-0.12) min for the apo form to 1.86 (+0.88/-0.45) min in the presence of ADP (Figure 2E). This significant slowing of NBD crosslinking supports our conclusion that ADP-bound hP-gp exists primarily in an open conformation.

Molecular Pharmacology Fast Forward. Published on May 11, 2016 as DOI: 10.1124/mol.116.104190
This article has not been copyedited and formatted. The final version may differ from this version.

Numerous crystal structures for ABC transporter family members have previously been reported; however, the majority of these are found in an open, "inward facing" conformation. Because the resolution of our cryo-EM maps is not sufficient to allow us to create a model for hP-gp directly, we have generated molecular envelopes by fitting existing models of ABC transporters into the density maps. The models that most resemble the open hP-gp cryo-EM conformations are those of mouse P-gp in the open, inward facing conformation (PDB IDs: 4M1M and 4KSC) (Li et al., 2014; Ward et al., 2013). By rigidly fitting each of these into the open conformation of apo EQ hP-gp (Figure 3A, B), and into the open structure of WT-ADP hP-gp with the greatest distance (Figure 3E, F) or least distance (Figure 3C, D) between NBDs, we can see that the previously determined open conformations for mouse P-gp closely match the spectrum of open conformations that we have observed. A quantitation of the relative fit of each of these models into our maps suggests that the 4KSC mouse P-gp structure fits better to the apo open state or to the open conformation of hPgp•ADP with greater distance between the NBDs, while the 4M1M mouse P-gp model is a better match for the structure of hPgp•ADP with the least distance between NBDs (Figure 3J).

We fit the EQ apo closed map with the only available structures reported to be of an occluded or outward-facing conformation, those of McjD (PDB 4PLO) from *E. coli* and Sav1866 (PBD 2HYD) from *S. aureus*, respectively, as well as the structure of mouse Pgp in the open conformation (PBD 4M1M, Figure 3G). As shown in Figure 3H-I, neither 4PLO or 2HYD adequately fit our closed structure, as the angles between the NBDs and the remainder of the protein are not consistent with our data. In contrast to the open (apo) conformation, none of the available crystal structures, including those reported to capture a closed state, show a good match

Molecular Pharmacology Fast Forward. Published on May 11, 2016 as DOI: 10.1124/mol.116.104190
This article has not been copyedited and formatted. The final version may differ from this version.

to the density map of the closed hP-gp form that we observe, suggesting that human P-gp exists in a unique conformation in its closed (outside open) state, which is different from reported closed conformations of other ABC transporters.

Discussion

The ATPase cycle of mammalian P-gp has been biochemically well characterized (Al-Shawi, 2011; Sauna and Ambudkar, 2007; Sharom, 2014). The reaction cycle is same in the absence or presence of transport substrate except that substrates alter the maximal velocity without affecting the K_m for ATP (Ambudkar et al., 1992; Sarkadi et al., 1992). The substrates or modulators affect the rate of ADP release, as this is the rate-limiting step in the ATP hydrolysis cycle (Kerr et al., 2001). In this study, we have used cryo-EM to analyze the conformational landscape of the hP-gp ATPase cycle (Figure 4), demonstrating a dynamic equilibrium between an open conformation and a novel closed conformation in the nucleotide-free and pre-hydrolytic ATP-bound states. Following ATP hydrolysis, and the subsequent release of phosphate (due to its significantly lower affinity (Urbatsch et al., 1995)), the hP-gp•ADP complex is predominantly in an open, 'inward facing' conformation. Upon dissociation of ADP from the catalytic site, hP-gp is reset for the next cycle. At the current resolution of these maps, we cannot unequivocally demonstrate whether the open and closed conformations correspond to "inward-facing" or "outward-facing" in the TMD. Nevertheless, we have previously shown that the ADP•Vi bound state is an "outward-facing" conformation, as this post-hydrolysis state has relatively low affinity for drug substrate (Sauna and Ambudkar, 2000), suggesting that the "closed" conformation observed here is "outward-facing", and that the open conformations are "inward-facing". While substrate-binding to the drug-binding pocket in the TM region is not required for the basal

Molecular Pharmacology Fast Forward. Published on May 11, 2016 as DOI: 10.1124/mol.116.104190
This article has not been copyedited and formatted. The final version may differ from this version.

ATPase activity, the discovery of the uniformly closed conformation in the post-hydrolytic state and the predominantly open conformation in the ADP-bound state also supports the findings that drug-substrate transport is coupled to ATPase activity (Ambudkar et al., 1997).

The presence of possible pseudosymmetry in certain projection views could be a source for misalignment, thereby limiting map resolution. In addition, it is possible that the presence of UIC2 antibody and our use of detergent micelles may influence the relative proportion of molecules in each state in our structural analysis. Further structural studies of hP-gp in a native membrane environment may shed more light on whether antibody binding affects the equilibrium between open and closed conformations. Nevertheless, the conformational heterogeneity we report here is consistent with earlier findings, and potentially explains the apparently conflicting results reported previously with various other members of the ABC transporter family. For example, the ATP analog (AMP-PMP)-bound form of the *S. aureus* transporter Sav1866 was reported to be present in an outward-facing conformation (Dawson and Locher, 2006), while that of the mitochondrial transporter ABCB10 bound to AMP-PMP was reported to be present in an inward-facing conformation (Shintre et al., 2013). For the bacterial heterodimeric ABC transporter TM287/288, NBDs were observed in close contact (but still in an inward-facing conformation) in the presence or absence of AMPPNP, which is expected to be analogous to ATP (Hohl et al., 2014). Similarly, a recent study suggested that a bacterial ABC lipid-linked oligosaccharide flippase (PglK) can adopt an inward-facing conformation in the absence of nucleotide, and an outward-facing conformation in the presence of ATP *in vitro*, generating a “futile cycle”. Nevertheless, the functional state required for flippase activity was found to be only the outward-facing state (see Figure 5 in Perez *et al.* (2015) (Perez et al.,

Molecular Pharmacology Fast Forward. Published on May 11, 2016 as DOI: 10.1124/mol.116.104190
This article has not been copyedited and formatted. The final version may differ from this version.

2015)). We propose that the equilibrium between the inward- and outward facing conformations may vary for different transporters, thus rationalizing these seemingly divergent observations across various members of this protein family.

Acknowledgements:

We thank Drs. Jason Pierson and Lingbo Yu for assistance with data collection, Michael Maurizi and Mr. Luke Diorio for help with separation of nucleotides, Dr. Soojay Banerjee for many helpful discussions, George Leiman for assistance in preparing the manuscript, and Veronica Falconieri for assistance with preparing the schematic illustration. This study utilized the computational resources of the NIH HPC Biowulf cluster (http://hpc.nih.gov). The density maps presented here have been deposited with the Electron Microscopy Data Bank (accession numbers EMD-3421, 3422, 3423, 3424, 3425, 3426, 3427, 3428, 3429, and 3430), and the refined atomic model for UIC2 has been deposited in the Protein Data Bank (accession number PDB-5JUE).
Address for correspondence: ambudkar@helix.nih.gov (Suresh V. Ambudkar) or ss1@nih.gov (Sriram Subramaniam).

Author Contributions:

Participated in research design: Frank, Shukla, Ambudkar, and Subramaniam

Conducted experiments: Frank, Shukla, Rao, Merk and Mobin

Performed data analysis: Frank, Shukla, Borgnia, Bartesaghi, Ambudkar, and Subramaniam

Contributed reagents and discussion: Esser, Gottesman, and Xia

Molecular Pharmacology Fast Forward. Published on May 11, 2016 as DOI: 10.1124/mol.116.104190
This article has not been copyedited and formatted. The final version may differ from this version.

Wrote the paper: Frank, Shukla, Earl, Ambudkar, and Subramaniam

Molecular Pharmacology Fast Forward. Published on May 11, 2016 as DOI: 10.1124/mol.116.104190
This article has not been copyedited and formatted. The final version may differ from this version.

References:

Al-Shawi MK (2011) Catalytic and transport cycles of ABC exporters. *Essays Biochem* **50**(1): 63-83.

Aller SG, Yu J, Ward A, Weng Y, Chittaboina S, Zhuo R, Harrell PM, Trinh YT, Zhang Q, Urbatsch IL and Chang G (2009) Structure of P-glycoprotein reveals a molecular basis for poly-specific drug binding. *Science* **323**(5922): 1718-1722.

Ambudkar SV (1998) Drug-stimulatable ATPase activity in crude membranes of human MDR1-transfected mammalian cells. *Methods Enzymol* **292**: 504-514.

Ambudkar SV, Cardarelli CO, Pashinsky I and Stein WD (1997) Relation between the turnover number for vinblastine transport and for vinblastine-stimulated ATP hydrolysis by human P-glycoprotein. *J Biol Chem* **272**(34): 21160-21166.

Ambudkar SV, Dey S, Hrycyna CA, Ramachandra M, Pastan I and Gottesman MM (1999) Biochemical, cellular, and pharmacological aspects of the multidrug transporter. *Annu Rev Pharmacol Toxicol* **39**: 361-398.

Ambudkar SV, Lelong IH, Zhang J, Cardarelli CO, Gottesman MM and Pastan I (1992) Partial purification and reconstitution of the human multidrug-resistance pump: characterization of the drug-stimulatable ATP hydrolysis. *Proc Natl Acad Sci U S A* **89**(18): 8472-8476.

Bartesaghi A, Matthies D, Banerjee S, Merk A and Subramaniam S (2014) Structure of beta-galactosidase at 3.2-A resolution obtained by cryo-electron microscopy. *Proc Natl Acad Sci U S A* **111**(32): 11709-11714.

Choudhury HG, Tong Z, Mathavan I, Li Y, Iwata S, Zirah S, Rebuffat S, van Veen HW and Beis K (2014) Structure of an antibacterial peptide ATP-binding cassette transporter in a novel outward occluded state. *Proc Natl Acad Sci U S A* **111**(25): 9145-9150.

Dawson RJ and Locher KP (2006) Structure of a bacterial multidrug ABC transporter. *Nature* **443**(7108): 180-185.

Hohl M, Hurlimann LM, Bohm S, Schoppe J, Grutter MG, Bordignon E and Seeger MA (2014) Structural basis for allosteric cross-talk between the asymmetric nucleotide binding sites of a heterodimeric ABC exporter. *Proc Natl Acad Sci U S A* **111**(30): 11025-11030.

Jin MS, Oldham ML, Zhang Q and Chen J (2012) Crystal structure of the multidrug transporter P-glycoprotein from Caenorhabditis elegans. *Nature* **490**(7421): 566-569.

Kerr KM, Sauna ZE and Ambudkar SV (2001) Correlation between steady-state ATP hydrolysis and vanadate-induced ADP trapping in Human P-glycoprotein. Evidence for ADP release as the rate-limiting step in the catalytic cycle and its modulation by substrates. *J Biol Chem* **276**(12): 8657-8664.

Kim J, Wu S, Tomasiak TM, Mergel C, Winter MB, Stiller SB, Robles-Colmanares Y, Stroud RM, Tampe R, Craik CS and Cheng Y (2015) Subnanometre-resolution electron cryomicroscopy structure of a heterodimeric ABC exporter. *Nature* **517**(7534): 396-400.

Li J, Jaimes KF and Aller SG (2014) Refined structures of mouse P-glycoprotein. *Protein Sci* **23**(1): 34-46.

Loo TW, Bartlett MC, Detty MR and Clarke DM (2012) The ATPase activity of the P-glycoprotein drug pump is highly activated when the N-terminal and central regions of the nucleotide-binding domains are linked closely together. *J Biol Chem* **287**(32): 26806-26816.

Mechetner EB, Schott B, Morse BS, Stein WD, Druley T, Davis KA, Tsuruo T and Roninson IB (1997) P-glycoprotein function involves conformational transitions detectable by differential immunoreactivity. *Proc Natl Acad Sci U S A* **94**(24): 12908-12913.

Mindell JA and Grigorieff N (2003) Accurate determination of local defocus and specimen tilt in electron microscopy. *J Struct Biol* **142**(3): 334-347.

Moeller A, Lee SC, Tao H, Speir JA, Chang G, Urbatsch IL, Potter CS, Carragher B and Zhang Q (2015) Distinct conformational spectrum of homologous multidrug ABC transporters. *Structure* **23**(3): 450-460.

Perez C, Gerber S, Boilevin J, Bucher M, Darbre T, Aebi M, Reymond J-L and Locher KP (2015) Structure and mechanism of an active lipid-linked oligosaccharide flippase. *Nature* **524**(7566): 433-438.

Pettersen EF, Goddard TD, Huang CC, Couch GS, Greenblatt DM, Meng EC and Ferrin TE (2004) UCSF Chimera--a visualization system for exploratory research and analysis. *J Comput Chem* **25**(13): 1605-1612.

Ramachandra M, Ambudkar SV, Gottesman MM, Pastan I and Hrycyna CA (1996) Functional characterization of a glycine 185-to-valine substitution in human P-glycoprotein by using a vaccinia-based transient expression system. *Mol Biol Cell* **7**(10): 1485-1498.

Ritchie TK, Kwon H and Atkins WM (2011) Conformational analysis of human ATP-binding cassette transporter ABCB1 in lipid nanodiscs and inhibition by the antibodies MRK16 and UIC2. *J Biol Chem* **286**(45): 39489-39496.

Sarkadi B, Price EM, Boucher RC, Germann UA and Scarborough GA (1992) Expression of the human multidrug resistance cDNA in insect cells generates a high activity drug-stimulated membrane ATPase. *J Biol Chem* **267**(7): 4854-4858.

Sauna ZE and Ambudkar SV (2000) Evidence for a requirement for ATP hydrolysis at two distinct steps during a single turnover of the catalytic cycle of human P-glycoprotein. *Proc Natl Acad Sci U S A* **97**(6): 2515-2520.

Sauna ZE and Ambudkar SV (2007) About a switch: how P-glycoprotein (ABCB1) harnesses the energy of ATP binding and hydrolysis to do mechanical work. *Mol Cancer Ther* **6**(1): 13-23.

Sauna ZE, Kim IW, Nandigama K, Kopp S, Chiba P and Ambudkar SV (2007) Catalytic cycle of ATP hydrolysis by P-glycoprotein: evidence for formation of the E.S reaction intermediate with ATP-gamma-S, a nonhydrolyzable analogue of ATP. *Biochemistry* **46**(48): 13787-13799.

Sauna ZE, Nandigama K and Ambudkar SV (2006) Exploiting reaction intermediates of the ATPase reaction to elucidate the mechanism of transport by P-glycoprotein (ABCB1). *J Biol Chem* **281**(36): 26501-26511.

Scheres SH (2012) RELION: implementation of a Bayesian approach to cryo-EM structure determination. *J Struct Biol* **180**(3): 519-530.

Senior AE (2011) Reaction chemistry ABC-style. *Proc Natl Acad Sci U S A* **108**(37): 15015-15016.

Sharom FJ (2014) Complex Interplay between the P-Glycoprotein Multidrug Efflux Pump and the Membrane: Its Role in Modulating Protein Function. *Front Oncol* **4**: 41.

Shintre CA, Pike AC, Li Q, Kim JI, Barr AJ, Goubin S, Shrestha L, Yang J, Berridge G, Ross J, Stansfeld PJ, Sansom MS, Edwards AM, Bountra C, Marsden BD, von Delft F, Bullock AN, Gileadi O, Burgess-Brown NA and Carpenter EP (2013) Structures of ABCB10, a human ATP-binding cassette transporter in apo- and nucleotide-bound states. *Proc Natl Acad Sci U S A* **110**(24): 9710-9715.

Sim HM, Bhatnagar J, Chufan EE, Kapoor K and Ambudkar SV (2013) Conserved Walker A cysteines 431 and 1074 in human P-glycoprotein are accessible to thiol-specific agents in the apo and ADP-vanadate trapped conformations. *Biochemistry* **52**(41): 7327-7338.

Szewczyk P, Tao H, McGrath AP, Villaluz M, Rees SD, Lee SC, Doshi R, Urbatsch IL, Zhang Q and Chang G (2015) Snapshots of ligand entry, malleable binding and induced helical movement in P-glycoprotein. *Acta Crystallogr D Biol Crystallogr* **71**(Pt 3): 732-741.

Tang G, Peng L, Baldwin PR, Mann DS, Jiang W, Rees I and Ludtke SJ (2007) EMAN2: an extensible image processing suite for electron microscopy. *J Struct Biol* **157**(1): 38-46.

Urbatsch IL, Sankaran B, Weber J and Senior AE (1995) P-glycoprotein is stably inhibited by vanadate-induced trapping of nucleotide at a single catalytic site. *J Biol Chem* **270**(33): 19383-19390.

Ward AB, Szewczyk P, Grimard V, Lee CW, Martinez L, Doshi R, Caya A, Villaluz M, Pardon E, Cregger C, Swartz DJ, Falson PG, Urbatsch IL, Govaerts C, Steyaert J and Chang G (2013) Structures of P-glycoprotein reveal its conformational flexibility and an epitope on the nucleotide-binding domain. *Proc Natl Acad Sci U S A* **110**(33): 13386-13391.

Wilkens S (2015) Structure and mechanism of ABC transporters. *F1000Prime Rep* **7**: 14.

Molecular Pharmacology Fast Forward. Published on May 11, 2016 as DOI: 10.1124/mol.116.104190
This article has not been copyedited and formatted. The final version may differ from this version.

Footnotes: This work was supported by funds from the Intramural Research Program of the National Institutes of Health, National Cancer Institute, Center for Cancer Research, the NIH-FEI Living Laboratory for Structural Biology, and the Center for Cancer Research Center for Molecular Microscopy.

Gabriel A. Frank and Suneet Shukla contributed equally to this work.

Reprint requests may be sent to Sriram Subramaniam; ss1@nih.gov. Mailing address: 50 South Drive, Rm 4306; Bethesda, MD 20892.

Molecular Pharmacology Fast Forward. Published on May 11, 2016 as DOI: 10.1124/mol.116.104190
This article has not been copyedited and formatted. The final version may differ from this version.

Figure Legends:

Figure 1: Cryo-EM analysis of nucleotide-free and ATP-bound pre-hydrolytic states of hP-gp. (A) Purified P-gp (2 μg protein) was separated on a 7% Tris-acetate gel and detected by silver stain (left panel) or Western blot analysis (right panel) using the C219 antibody. The protein gel and the Western blot are representative of four independent experiments. (B) 2 μg Purified Fab, hP-gp and hP-gp-Fab complex were separated on a native 4-16% Bis-Tris gel and stained with colloidal blue stain. Lanes display molecular weight standards (lane 1), purified UIC2 Fab fragment (lane 2), purified hP-gp (lane 3), and hP-gp-Fab complex (lane 4). The native gel is representative of three independent experiments. (C) A representative micrograph of EQ mutant hP-gp in the apo (nucleotide-free) state taken at an approximate defocus value of -3.4 μm. Selected front and side view projections of the protein are indicated with black and white circles, respectively. Scale bar 500Å. (D) Representative 2D image classes from apo EQ-hP-gp bound to UIC2. The NBD regions in the classes display variations in arrangement relative to the bound Fab, with the NBDs closer in some and further apart in others (bottom two red squares). (E-F) 3D cryo-EM reconstructions of hP-gp bound to UIC2 antibody, in open (E) and closed (F) conformations. (G-J) The EQ-hP-gp mutant displays open (G, I), and closed (H, J) conformations in both apo (G, H) and in ATP-bound (I, J) states. All the maps we present here have resolutions of ~ 15Å based on the 0.5 FSC criterion from comparing two half-maps, and also display features consistent with cryo-EM density maps at this resolution (Supplementary Figure 1A).

Figure 2: Cryo-EM analysis of hP-gp in post-hydrolytic and ADP-bound states. (A) WT hP-gp bound to UIC2 and trapped with ADP•Vi in the post-hydrolytic state reveals only the closed

Molecular Pharmacology Fast Forward. Published on May 11, 2016 as DOI: 10.1124/mol.116.104190
This article has not been copyedited and formatted. The final version may differ from this version.

conformation, even with 3D classification. (B-D) WT hP-gp bound to UIC2 and incubated with 5 mM ADP is found in multiple open conformations, but not in the closed conformation. (E) WT hP-gp expressing crude membranes were incubated in absence (apo, circle, blue) or presence of 5 mM ADP (square, green) at 37°C for 10 min and $CuSO_4$ induced crosslinking was performed for the indicated times (x-axis). The extent of crosslinking expressed as a relative percentage (y-axis) was calculated by densitometric analysis of crosslinked P-gp band on Western blots. The error bars denote standard error (n=3), and the time required for 50% crosslinking (t½) was calculated by nonlinear regression analysis to an exponential decay using GraphPad Prism 6.0.

Figure 3: Cryo-EM reconstructions of open and closed conformations of hP-gp fit with X-ray crystallographic models. X-ray crystallographic models of mouse P-gp in the open conformation (PDB entries 4M1M and 4KSC) were fit into hP-gp cryo-EM density maps along with coordinates of the UIC2 Fab (obtained from X-ray crystallographic analysis; Shukla, Esser, Ambudkar and Xia, unpublished data) using the program Chimera (Pettersen et al., 2004). (A-B) Map of the nucleotide-free EQ hP-gp mutant in the open conformation fit with 4M1M (A) or 4KSC (B). (C-D) Map of WT hP-gp bound to ADP with most-separated NBDs fit with 4M1M (C) or 4KSC (D). (E-F) Map of WT hP-gp bound to ADP with least-separated NBDs fit with 4M1M (E) or 4KSC (F). (G-I) Map of WT hP-gp bound to ADP•Vi fit with 4M1M (G), the model of *S. aureus* ABC transporter sav1866 (PBD 2HYD, H), or the model of *E. coli* ABC transporter McjD (PBD 4PL0, I). (J) Quantitation of best fit of open conformations with 4M1M and 4KSC, showing the total percentage of atoms in the X-ray models that fall within the density of our cryo-EM derived map. Maps were identically thresholded to the volume of the UIC2 crystal structure filtered to 15Å resolution.

Molecular Pharmacology Fast Forward. Published on May 11, 2016 as DOI: 10.1124/mol.116.104190
This article has not been copyedited and formatted. The final version may differ from this version.

Figure 4: Schematic of hP-gp at major steps during the ATPase reaction cycle. Our data indicate that in the nucleotide state (top, dark blue), hP-gp exists in a dynamic equilibrium between open and closed conformations. Binding of ATP (right, orange) also allows both open and closed conformations. After hydrolysis of ATP to ADP•P_i (as trapped by ADP•V_i, bottom, purple), hP-gp is found exclusively in the closed conformation. Release of P_i allows the ADP-bound state of hP-gp (left, green) to open. The ADP-bound state is highly flexible, but remains in the open state. Release of ADP allows hP-gp to sample the closed conformation (top).

Molecular Pharmacology Fast Forward. Published on May 11, 2016 as DOI: 10.1124/mol.116.104190
This article has not been copyedited and formatted. The final version may differ from this version.

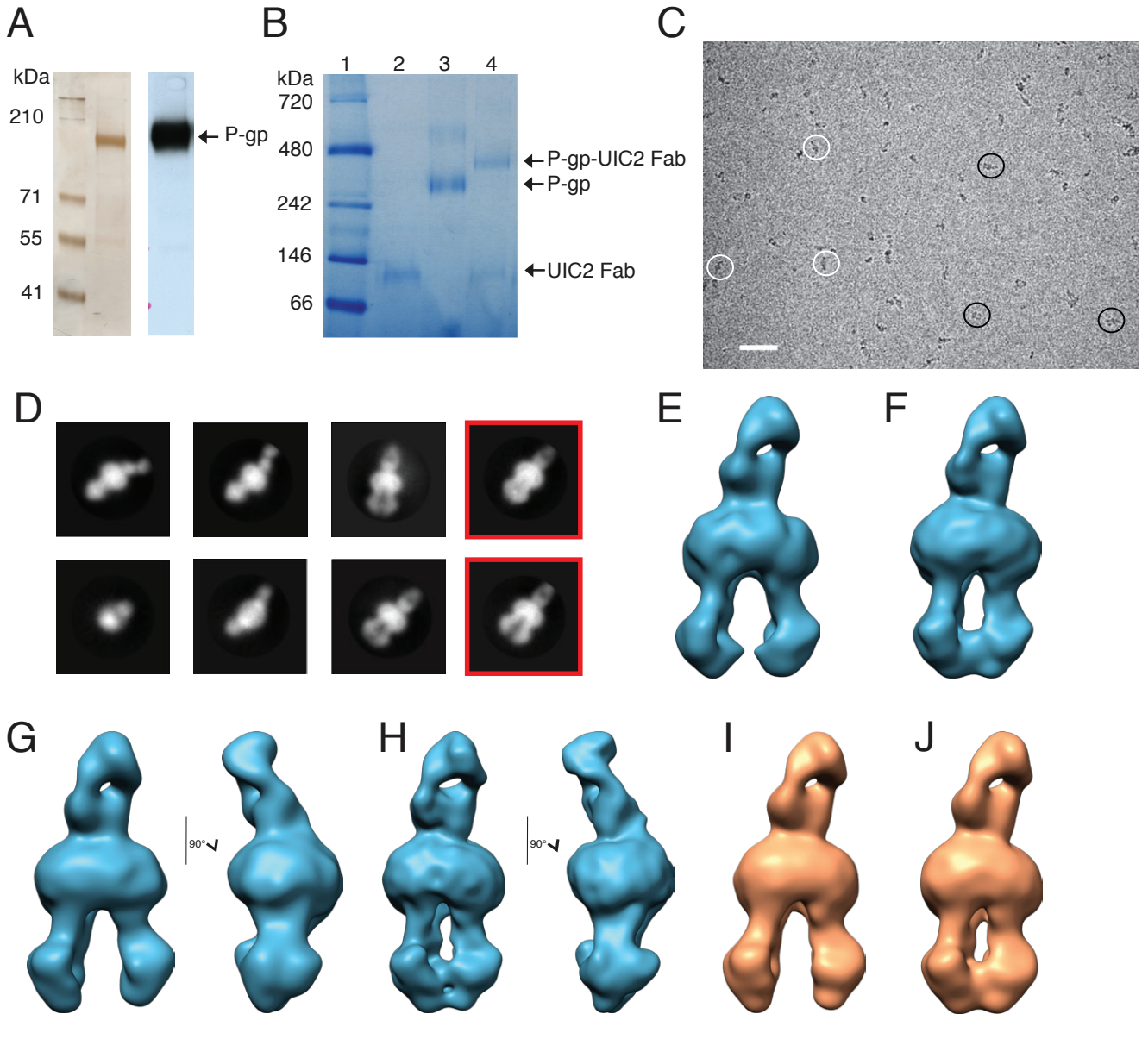

Figure 1

Molecular Pharmacology Fast Forward. Published on May 11, 2016 as DOI: 10.1124/mol.116.104190
This article has not been copyedited and formatted. The final version may differ from this version.

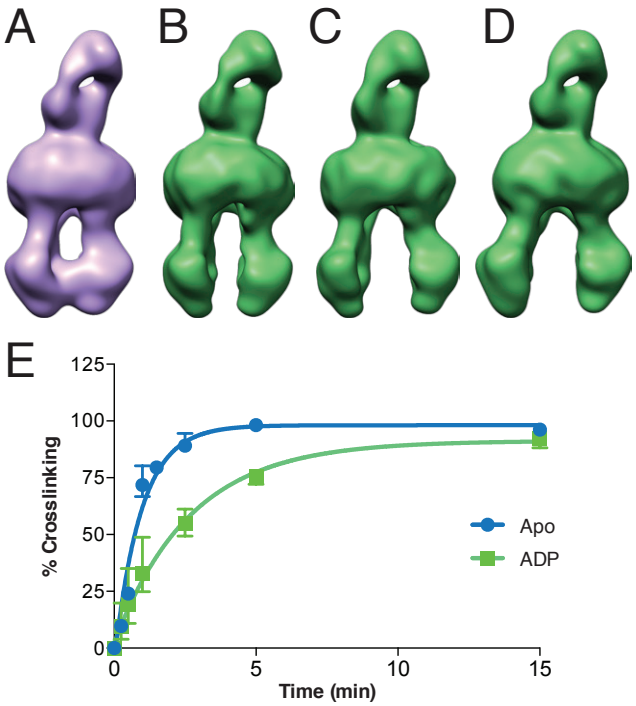

Figure 2

Molecular Pharmacology Fast Forward. Published on May 11, 2016 as DOI: 10.1124/mol.116.104190
This article has not been copyedited and formatted. The final version may differ from this version.

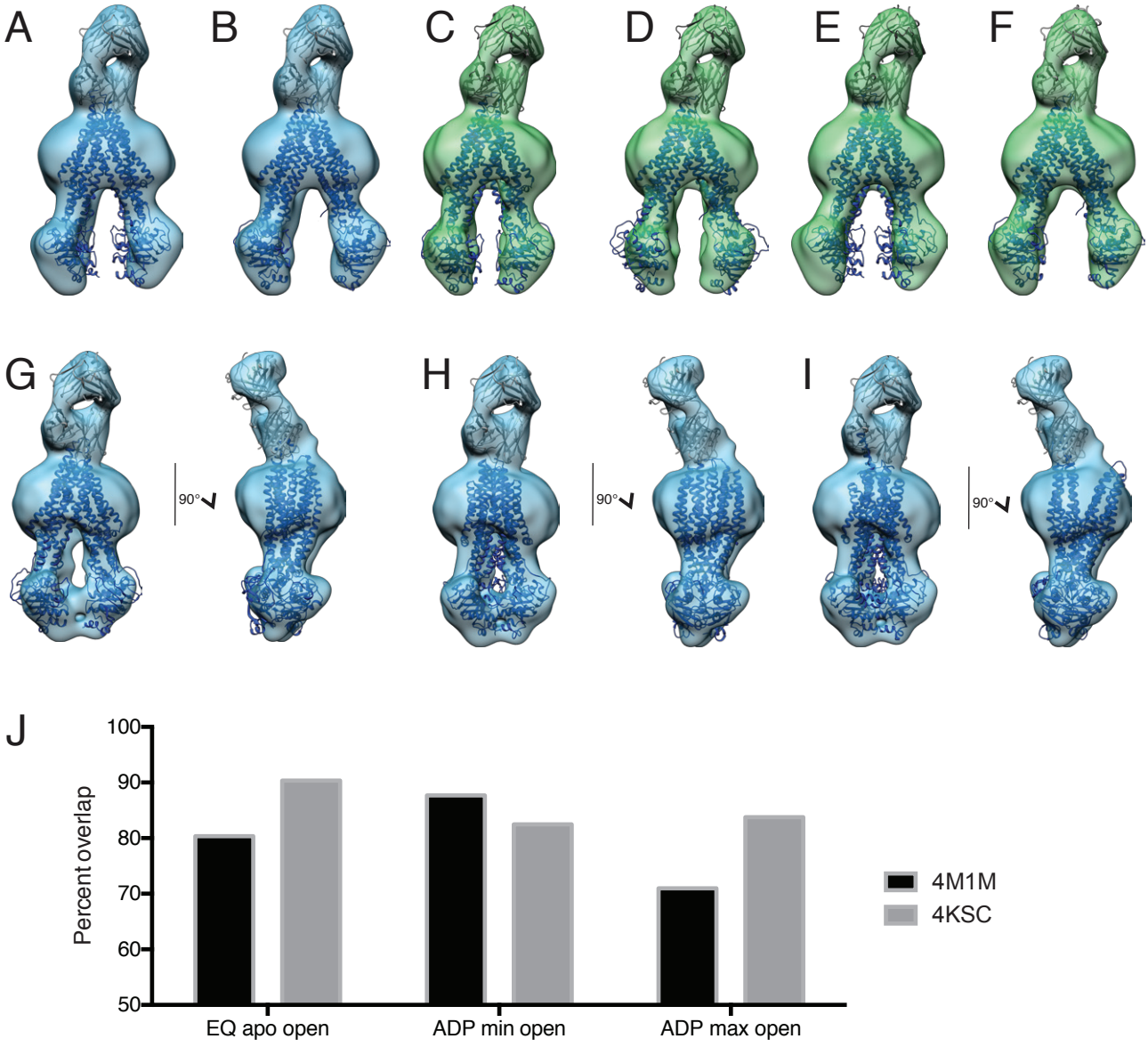

Figure 3

Molecular Pharmacology Fast Forward. Published on May 11, 2016 as DOI: 10.1124/mol.116.104190
This article has not been copyedited and formatted. The final version may differ from this version.

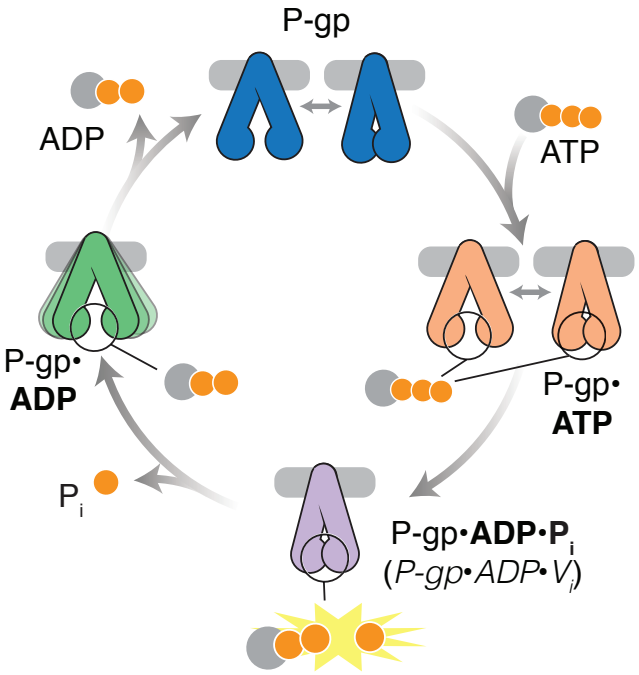

Figure 4